ADVANCED FUNCTIONAL MATERIALS
www.afm-journal.de

Three-Dimensionally Ordered Macroporous Polymeric Materials by Colloidal Crystal Templating for Reversible CO_2 Capture

*Hongkun He, Mingjiang Zhong, Dominik Konkolewicz, Karin Yacatto, Timothy Rappold, Glenn Sugar, Nathaniel E. David, Jeff Gelb, Naomi Kotwal, Arno Merkle, and Krzysztof Matyjaszewski**

The design and preparation of porous materials with controlled structures and functionalities is crucial to a variety of absorption- or separation-relevant applications, including CO_2 capture. Here, novel functional polymeric materials with three-dimensionally ordered macroporous (3DOM) structures are prepared by using colloidal crystals as templates using relatively simple, rapid, and inexpensive approaches. These ordered structures are used for the reversible CO_2 capture from ambient air by humidity swing. Typically, the colloidal crystal template is synthesized from polymer latex particles of poly(methyl methacrylate) (PMMA) or polystyrene (PS). To maintain the functionality of the material, it is important to prevent the porous structure collapsing, which can occur by the hydrolysis of the ester bonds in conventional crosslinkers under basic conditions. This hydrolysis can be prevented by using a water-soluble crosslinker containing two quaternary ammonium moieties, which can be used to prepare stable porous crosslinked polymers with the monomer (vinylbenzyl)trimethylammonium chloride (VBTMACl) and using a PMMA-based colloidal crystal template. The hydroxide-containing monomer and dicationic crosslinker are synthesized from their chloride precursors, avoiding the ion-exchange step which causes shrinkage of the pores. An analysis of different methods for infiltrating the monomer solution into the colloidal crystal template shows that infiltration using capillary forces leads to fewer defects than infiltration under a partial vacuum. In addition, functional macroporous films with micrometer thickness are prepared from a template of PS-based colloidal crystals in a thin film. In general, the colloidal crystal templated materials showed improved CO_2 absorption/desorption rates and swing sizes compared to a commercially available material with similar functional groups. This work could easily be extended to create a new generation of ordered macroporous polymeric materials with tunable functionalities for other applications.

1. Introduction

Colloidal crystals are three-dimensional (3D) periodic lattices formed from monodisperse spherical colloidal particles.[1] In a colloidal crystal, uniformly sized spheres are close packed in a predominantly face-centered cubic (fcc) crystalline structure, assembled by entropy-driven crystallization.[2] Colloidal crystals can be prepared from monodisperse polymeric or inorganic colloids as building blocks, which are typically polymer latex or silica microspheres. Because of their unique structures and properties, colloidal crystals have applications as photonic crystals,[3] sensors,[4] membranes,[5] and scaffolds for tissue engineering.[6]

Due to their unique structures, colloidal crystals have been used as templates for highly ordered porous polymeric structures in recent years.[7] The inverse polymer opals are formed in the interstitial sites of the colloidal crystal templates, giving a three-dimensionally ordered macroporous (3DOM) structure.[8] The preparation of periodic macroporous structures by colloidal crystal templating involves four steps: synthesis of colloidal spheres, preparation of the colloidal crystal template, precursor infiltration followed by polymerization, and template removal.[9] Various inorganic or polymeric particles can be used in the first step.[10] The second step involves the assembly of the spheres into a colloidal

H. He, M. Zhong, Dr. D. Konkolewicz, Prof. K. Matyjaszewski
Center for Macromolecular Engineering
Department of Chemistry
Carnegie Mellon University
Pittsburgh, PA 15213. USA
E-mail: km3b@andrew.cmu.edu

K. Yacatto, T. Rappold, G. Sugar, N. E. David
Kilimanjaro Energy, Inc., San Francisco, CA 94107, USA
J. Gelb, N. Kotwal, A. Merkle
Xradia, Inc., Pleasanton, CA 94588, USA

DOI: 10.1002/adfm.201300401

crystal, which can be achieved by various approaches, such as sedimentation,[11] centrifugation,[12] electrodeposition,[13] vertical deposition,[14] filtration,[15] and slit filling.[16] In the third step, various polymer precursors can be infiltrated into the silica-based colloidal crystals, including monomers that are subsequently polymerized thermally or under UV to form macroporous films of polystyrene (PS), poly(methyl methacrylate) (PMMA), or polyurethane.[17] Similar approaches can be used to create various porous polymer replicas, such as polymerized divinylbenzene (DVB) and ethylene glycol dimethylacrylate (EGDMA),[18] epoxy resins,[19] polydimethylsiloxane (PDMS) elastomers,[20] polyethylene using gaseous phase as the precursors by chemical vapor deposition,[21] or poly(carbazole) via colloidal template-assisted electropolymerization.[22] In the final step, latex or silica spheres are removed by selective dissolution in organic solvents or hydrofluoric acid, respectively.

Generally, three types of precursors are used for the infiltration in colloidal crystals to obtain polymer networks: 1) polymer solutions; 2) monomer solutions; and 3) monomer and crosslinker solutions. For the polymer solutions, only evaporation of the solvent is needed; while for the last two cases, in situ polymerization is needed to form polymer networks after infiltration. In the first two cases, the resulting polymer matrix is uncrosslinked, while crosslinked polymer networks can improve the mechanical properties and resistance to high temperature and solvents.[23] The previous studies used common polymers, monomers, or crosslinkers, and focused on the structural and physical properties of the resulting materials. In order to expand the utility of these 3DOM polymeric materials for a specific function, components should be tailored to the desired application.

Herein, we report the synthesis of functional polymeric materials with 3DOM structures using colloidal crystal templates for reversible CO_2 capture from ambient air. The rapid growth of CO_2 emissions from fossil fuel combustion is a major cause of the greenhouse effect, leading to global warming and climate change.[24] In recent years, significant effort has been devoted to developing technologies that can reduce the CO_2 concentration in the atmosphere, typically through the capture of CO_2 using "point-source capture" at large power plants,[25] or "air capture" where CO_2 is absorbed directly from ambient air.[26] The humidity swing has emerged as a promising air-capture method, since it uses a change in the humidity of the surrounding air to reversibly absorb and desorb CO_2 at ambient conditions by switching between the bicarbonate–carbonate species. At low humidity the bicarbonate species are favored and CO_2 absorption occurs, while at high humidity carbonate species are favored and CO_2 desorption occurs.[27] It is also possible for hydroxide anions to undergo a one-time CO_2 absorption to form bicarbonates, allowing the system to be started from the hydroxide state. To enhance the CO_2 capture performance by the humidity swing, we used colloidal crystal templates to create macroporous polymers containing quaternary ammonium hydroxide groups, which can be used for the humidity swing.

Colloidal crystals templates have two obvious advantages. Firstly, the macropores in the resulting structures are interconnected, aiding the gas diffusion through the pores. Secondly, the pores have a high packing density, increasing the capacity for the gas absorption. The colloidal crystal templated materials show improved CO_2 capture performances compared to a commercially available resin, which was used as a standard. To the best of our knowledge, this study, along with our previous work,[28] is the first reported case of CO_2 capture sorbents based on macroporous polymeric materials prepared using colloidal crystal templates. This work also developed a facile and versatile strategy for the synthesis of highly-ordered porous structures by using novel crosslinkers and functional monomers. This opens an avenue for the design and preparation of macroporous polymer networks with controlled functionality by colloidal crystals templating, which could be used in various future applications.

2. Results and Discussion

2.1. 3DOM Polymeric Materials by PMMA Colloidal Crystals Templating with Dimethacrylate or Bisacrylamide Crosslinkers

In the first step, the monodisperse poly(methyl methacrylate) (PMMA) spheres were synthesized by surfactant-free emulsion polymerization of MMA in water with an azo initiator (2,2′-azobis(2-amidinopropane) dihydrochloride, V50) at 75 °C.[29] To create the colloidal crystal template, the colloidal suspension was subjected to centrifugation and drying, inducing the PMMA latex spheres to form three-dimensionally ordered arrays. As shown in the scanning electron microscopy (SEM) images in **Figure 1**, the PMMA spheres have an average diameter of 480 nm with a narrow size distribution, and the spheres were close-packed into an fcc lattice. The colloidal crystals are predominantly fcc with a small fraction of hexagonal close-packing (hcp) or random close-packing (rcp) regions.[30] This phenomenon originates from the fact that fcc is entropically favored over hcp by approximately $0.005RT$ per mol.[31] The fcc component was induced by gravity and centrifuge-induced stresses, since only random stacking of hexagonally close-packed (rhcp) structure can form in microgravity.[32] The colloidal spheres in the colloidal crystals have a packing density of 0.74, which is the highest among the common crystal structures.[12]

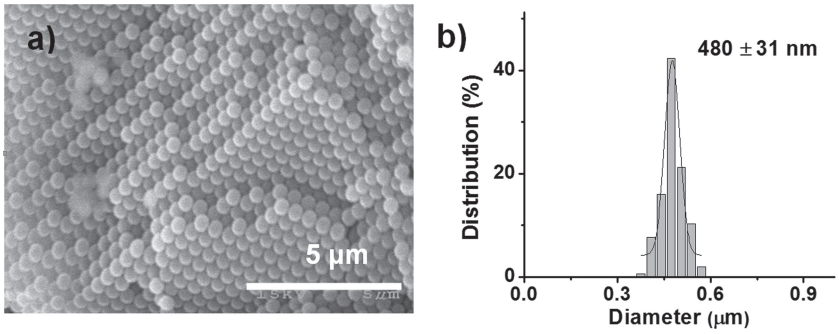

Figure 1. a) SEM image and b) the particle size histogram with a Gaussian size distribution fit (solid line) of PMMA colloidal crystals.

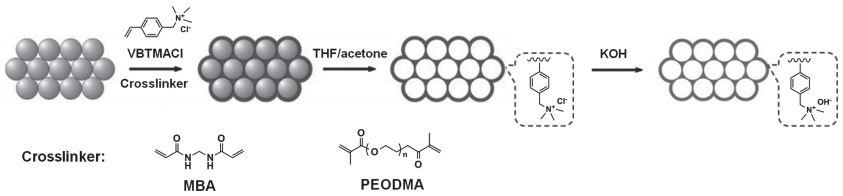

Scheme 1. Preparation of the 3DOM polymeric materials by PMMA colloidal crystals templating with VBTMACl and PEODMA/MBA.

In the third step of the preparation of the 3DOM polymeric materials, the PMMA colloidal crystals were used as the templates to create ordered macroporous polymeric materials, as shown in **Scheme 1**. First, the colloidal crystals were infiltrated with a mixture of the monomer (vinylbenzyl)trimethylammonium chloride (VBTMACl)), the water-soluble crosslinker (10% molar ratio to the monomer), as well as an azo initiator (2,2'-azobis[2-(2-imidazolin-2-yl)propane]dihydrochloride, VA-044). Initially, two water-soluble crosslinkers were used: *N,N*-methylenebis(acrylamide) (MBA) and poly(ethylene oxide) dimethacrylate (PEODMA, $\overline{M}_n$ = 750). The precursor mixture, in the void spaces formed between the PMMA spheres, was polymerized thermally at 80 °C.

In the final step, the PMMA spheres were removed by washing with tetrahydrofuran (THF) and acetone to generate the pores in the crosslinked polymer networks. The SEM images of the resulting uniform macroporous structures are shown in **Figure 2**. The white regions are the walls of the pores on the top layer, the gray regions are those in the second layer, and the dark regions are voids. The large pores have a size of ca. 0.5 μm, and the walls of the pores are formed by the crosslinked polymers. In each of the large pores, there are circular windows (ca. 50 nm in diameter) formed where the original PMMA spheres touched. The origin of the windows was attributed mainly to the fact that the PMMA spheres contacted each other so that the precursor solution did not penetrate those regions.[17c] In principle, each large pore should contain 12 small pores, since every sphere is in contact with 12 neighboring spheres in fcc packing.[9] In this structure, the windows connect neighboring macropores, making the whole material interconnected and increasing the porosity above 0.74.[19]

The crosslinked ordered macroporous polymers containing the quaternary ammonium chloride groups were treated with KOH in methanol to generate the quaternary ammonium hydroxide groups. After this treatment, the SEM images (Supporting Information, Figure S1a,c) showed the collapse of almost all of the original macropores. Two additional samples with a higher content of the crosslinker (50% molar ratio) were prepared, but their ordered macroporous structures still collapsed after KOH treatment (Supporting Information, Figure S1b,d). This collapse of the porous structure was caused by the hydrolysis of the ester or amide bonds in the crosslinkers under the highly basic conditions. To prevent the collapse of the pores, divinylbenzene (DVB) was also used as a crosslinker, since it contains no ester or amide bonds. However, after polymerization and removal of the templates, the pores collapsed (Supporting Information, Figure S2), and this pore collapse was also observed in three other control experiments, where the PMMA colloidal crystals were infiltrated with 4-chloromethyl styrene (CMS), DVB and methanol, respectively (Supporting Information, Figure S3). This was most likely caused by the PMMA spheres dissolving or swelling in the CMS, DVB, and methanol. Therefore, to preserve the porous structure, the polymer precursor solution should be aqueous with water-soluble monomers and stable crosslinkers that contain no ester or amide groups.

2.2. 3DOM Polymeric Materials by PMMA Colloidal Crystals Templating with VBTMACl and PMVPMACl

In order to obtain a stable water-soluble crosslinker, the esterification reactions that are usually used to prepare divinyl crosslinkers (e.g., starting from acrylic acid, methacrylic acid, etc.) should not be used due to hydrolysis. Thus, a styrene based water-soluble crosslinker should be prepared. The quaternization reaction between α,α'-dichloro-*p*-xylene and *N*-(4-vinylbenzyl)-*N,N*-dimethylamine was developed to produce a novel dicationic crosslinker, *N,N*]. Gelb-(1,4-phenylenebis(methylene))bis(*N,N*-dimethyl-1-(4-vinylphenyl) methanammonium) dichloride (PMVPMACl) (**Figure 3** and Supporting Information, Part D). The advantages of using this dicationic crosslinker are: 1) the dicationic crosslinker is very stable under highly alkaline conditions; 2) the molecule is water-soluble; 3) the synthetic procedure is facile and effective; and 4) the quaternary ammonium chloride groups can be transformed into quaternary ammonium hydroxide groups, which can be used for the humidity swing.

Four samples with different degrees of crosslinking were prepared using the dicationic crosslinker PMVPMACl and subjected to ion-exchange with KOH in methanol or water (**Scheme 2**). After ion-exchange, approximately 70–90% of the chlorine ions were converted to hydroxide ions, as determined from the elemental analysis of the chlorine content (Supporting Information, Table S1). As shown in the SEM images (**Figure 4** and Supporting Information, Figure S10–S13), for the samples with 10% crosslinker, the ordered macroporous structures partially

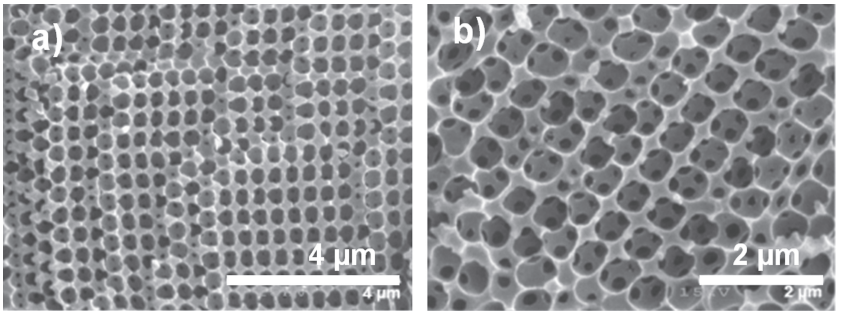

Figure 2. SEM images of the 3DOM polymeric materials by PMMA colloidal crystal templating with a) MBA or b) PEODMA as the crosslinker.

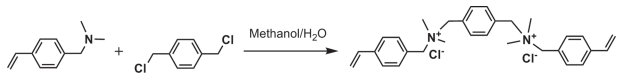

Figure 3. Synthesis of the dicationic crosslinker PMVPMACl.

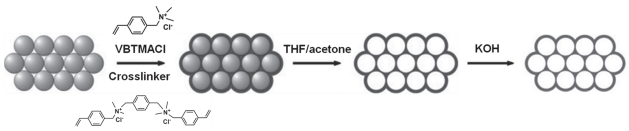

Scheme 2. Preparation of the 3DOM polymeric materials by PMMA colloidal crystals templating with VBTMACl and PMVPMACl.

collapsed, indicating that 10% crosslinker was insufficient to form rigid pore walls. For the samples with 20%, 50%, and 100% crosslinker, the ordered macroporous structure was well preserved after ion exchange. The large pores in these 3DOM crosslinked polymers were interconnected by circular windows. Also, most samples showed some shrinkage of the pores after ion exchange, for example, the sample with 20% crosslinker showed a decrease in the large pores from ca. 460 to 370 nm, and the windows decreased from ca. 220 to 70 nm after KOH treatment. The shrinkage of the pores, observed after ion exchange, was most likely due to the swelling and deformation of the crosslinked scaffolds in the KOH methanol/water solutions.

The CO_2 capture measurements were performed by placing the materials in a sealed chamber and recording CO_2 desorption and absorption kinetics when they were sequentially exposed to humid and dry conditions (specific humidity of 20 and 5 parts per thousand (ppt), which corresponds to approximately 90% and 20% relative humidity, respectively, at 20 °C). The CO_2 capture results for the 3DOM polymeric materials with different crosslinking degrees are shown in **Table 1** (entry 2–9), and their CO_2 absorption/desorption profiles are shown in the Supporting Information, Figure S17–S20. The commercially available Excellion membrane containing quaternary ammonium hydroxide groups was selected as the reference material.[27b,28] All these 3DOM polymeric materials had larger swing sizes (1.5–2.8-fold) and absorption/desorption rates (1.2–5.2-fold) compared to this standard, and they basically ranked from highest to lowest for the samples with crosslinking degrees of 20%, 50%, 10%, and 100%. The outperformance of the 3DOM polymeric materials over the Excellion membrane is mainly attributed to their interconnected macro porous structures, which provide larger surface areas and facilitate the diffusion of gases.

The relatively poor performance of the sample with 100% crosslinking could be due to the fact that the solubility of PMVPMACl in water is not as high as that of VBTMACl, and the precursor solutions have higher viscosity, which influences the infiltration process. For the sample with 10% crosslinks, the crosslinking density is too low to form a sufficiently strong crosslinked network, which results in partial collapse of the macropores.

Table 1. The CO_2 capture results for the 3DOM polymeric materials prepared by colloidal crystal templating.

Entry	Template[a]/Monomer/crosslinker/KOH treatment[b]/crosslinking degree[c]	Swing size [mmol g^{-1}]	Absorption rate [mmol min^{-1} g^{-1}]	Desorption rate [mmol min^{-1} g^{-1}]	Overall rate[d] [mmol min^{-1} g^{-1}]
1	Excellion membrane[f]	1.3×10^{-1}	4.0×10^{-3}	4.5×10^{-3}	2.1×10^{-3}
2	PMMA-CC/VBTMACl/PMVPMACl/W/10%	2.4×10^{-1}	5.0×10^{-3}	1.0×10^{-2}	3.4×10^{-3}
3	PMMA-CC/VBTMACl/PMVPMACl/M/10%	2.5×10^{-1}	6.2×10^{-3}	1.0×10^{-2}	3.9×10^{-3}
4	PMMA-CC/VBTMACl/PMVPMACl/W/20%	2.3×10^{-1}	4.3×10^{-3}	7.7×10^{-3}	2.7×10^{-3}
5[e]	PMMA-CC/VBTMACl/PMVPMACl/M/20%	3.7×10^{-1}	2.8×10^{-2}	1.8×10^{-2}	1.1×10^{-2}
6	PMMA-CC/VBTMACl/PMVPMACl/W/50%	3.3×10^{-1}	2.5×10^{-2}	1.6×10^{-2}	9.7×10^{-3}
7	PMMA-CC/VBTMACl/PMVPMACl/M/50%	2.7×10^{-1}	1.8×10^{-2}	1.2×10^{-2}	7.2×10^{-3}
8	PMMA-CC/VBTMACl/PMVPMACl/W/100%	1.9×10^{-1}	5.5×10^{-3}	8.0×10^{-3}	3.2×10^{-3}
9	PMMA-CC/VBTMACl/PMVPMACl/M/100%	2.4×10^{-1}	4.0×10^{-3}	7.3×10^{-3}	2.6×10^{-3}
10[f]	PMMA-CC/VBTMAOH/PMVPMAOH/-/20%	2.7×10^{-1}	1.0×10^{-2}	1.6×10^{-2}	6.3×10^{-3}
11[f]	PMMA-CC/VBTMAOH/PMVPMAOH/-/50%	2.1×10^{-1}	1.2×10^{-2}	1.5×10^{-2}	6.7×10^{-3}
12[g]	PMMA-CC/VBTMAOH/PMVPMAOH/-/20%	4.1×10^{-1}	5.2×10^{-3}	1.2×10^{-2}	3.6×10^{-3}
13	PS-CC-film/VBTMACl/PMVPMACl/M/20%	5.7×10^{-1}	6.4×10^{-3}	1.4×10^{-2}	4.4×10^{-3}

[a]Template: PMMA-CC = poly(methyl methacrylate) colloidal crystals; PS-CC-film = polystyrene colloidal crystals films; [b]KOH Treatment: "W" = KOH aqueous solution (1.2 g mL^{-1}); "M" = KOH/methanol solution (0.2 g mL^{-1}); "-" = no treatment; [c]Crosslinking degree: the molar ratio of the crosslinker to the monomer; [d]The overall rate is determined by: $\frac{1}{\text{overall rate}}=\frac{1}{\text{absorption rate}}+\frac{1}{\text{desorption rate}}$; [e]The data are taken from ref. [28]; [f]Using the infiltration method by filtration; [g]Using the infiltration method by capillary force.

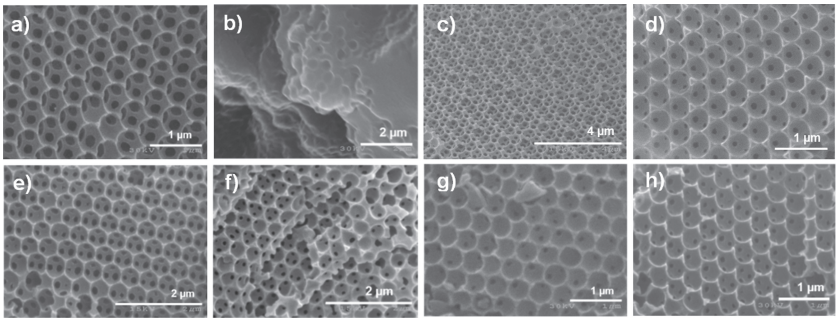

Figure 4. SEM images of the 3DOM polymeric materials prepared by PMMA colloidal crystal templating with VBTMACl and PMVPMACl with crosslinking degrees of a,b) 10%, c,d) 20%, e,f) 50%, and g,h) 100%: a,c,e,g) after removal of the templates by washing with THF/acetone; and, b,d,f,h) after ion-exchange with KOH/methanol solution.

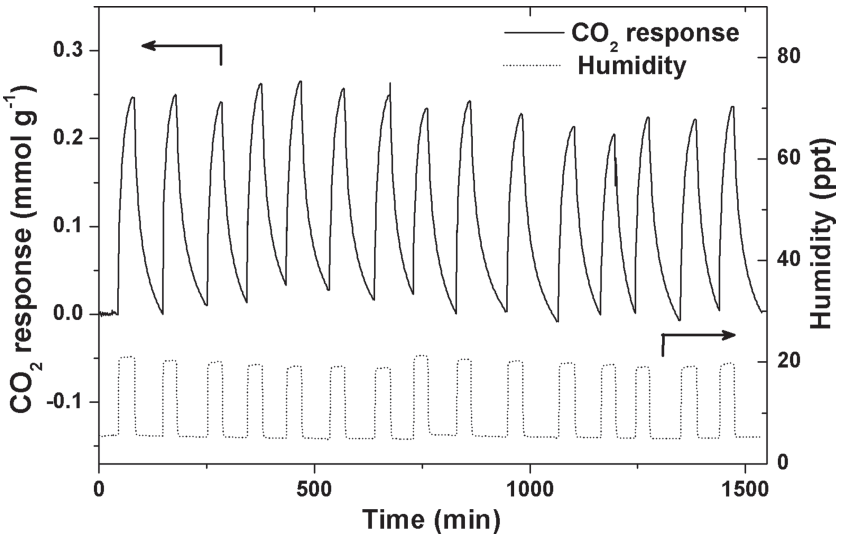

Figure 5. CO_2 absorption/desorption profiles (15 cycles) for the 3DOM polymeric materials by PMMA colloidal crystals templating with VBTMACl and PMVPMACl (20% mole ratio).

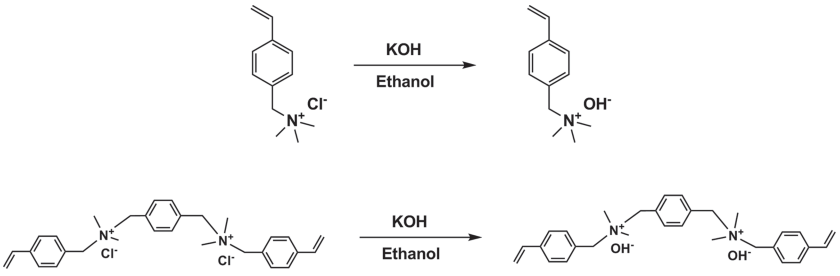

Figure 6. Synthesis of the hydroxide-containing monomer VBTMAOH and the hydroxide-containing dicationic crosslinker PMVPMAOH.

The humidity swing for CO_2 absorption/desorption was run for 15 cycles for the sample with 20% crosslinking degree, and essentially no decrease in the performance was observed (**Figure 5**), which suggests that the material is highly stable.

2.3. 3DOM Polymeric Materials by PMMA Colloidal Crystals Templating with VBTMAOH and PMVPMAOH

Since the KOH treatment shrank the pores of the 3DOM polymeric materials, it is desirable to polymerize the hydroxide-containing monomer and crosslinker. This avoids the ion-exchange step, which should reduce the shrinkage and increase the fraction of quaternary ammonium hydroxide groups in the resulting polymer. Simple reactions were developed to produce the hydroxide-containing monomer and dicationic crosslinker by reacting their chloride precursors with KOH in ethanol (**Figure 6** and Supporting Information, Part E).

Two samples with different crosslinking degrees were prepared from a PMMA colloidal crystals template with the hydroxide-containing monomer and dicationic crosslinker (**Scheme 3**). The SEM and thin-section TEM images (**Figure 7**) show that the ordered porous structure was preserved very well after removal of the PMMA templates without obvious collapse or distortion. The samples prepared from the hydroxide-containing precursors have larger pore sizes (420 and 100 nm for the macropores and windows, respectively) than the earlier samples prepared from chloride containing precursors followed by ion-exchange, which confirms that the pores shrank during the ion-exchange step.

The CO_2 capture results in Table 1 (entry 10–11) and Supporting Information (Figure S21) showed that the samples with 20% and 50% crosslinking degrees had a 2-fold increase in the swing size, and a 3-fold increase in the overall rate, compared to the Excellion membrane. These results are similar to those for the previous samples containing VBTMACl/PMVPMACl after ion-exchange, revealing that the ion-exchange step has minimal influence on the CO_2 capture results.

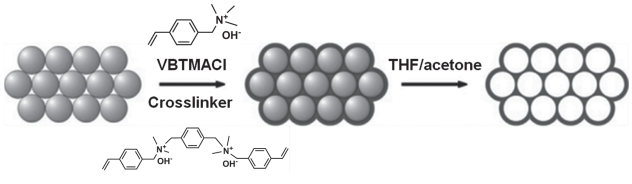

Scheme 3. Preparation of the 3DOM polymeric materials by PMMA colloidal crystals templating with VBTMAOH and PMVPMAOH.

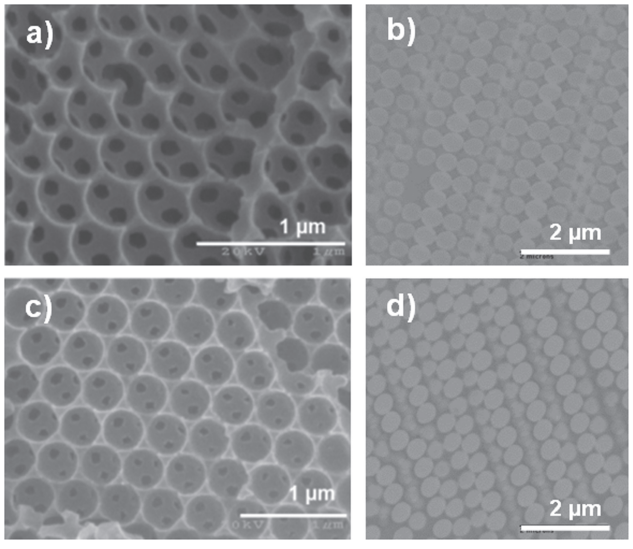

Figure 7. a,c) SEM and b,d) thin-section TEM images of the 3DOM polymeric materials prepared by PMMA colloidal crystal templating with VBTMAOH and PMVPMAOH without ion-exchange step using different crosslinking degrees: a,b) 20%, and, c,d) 50%.

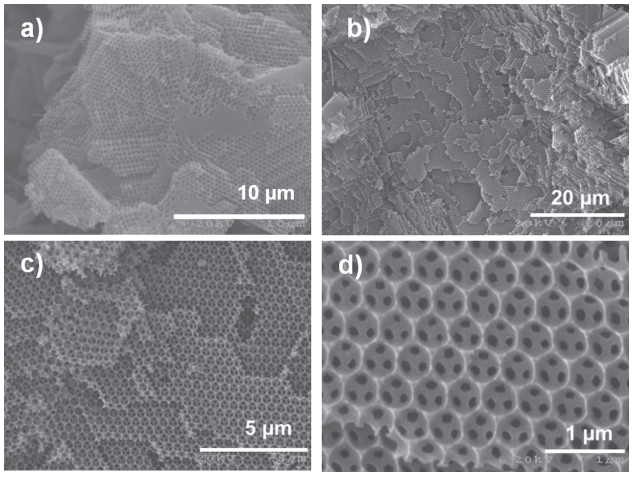

Figure 8. SEM images of the 3DOM polymeric materials prepared by PMMA colloidal crystal templating with VBTMAOH and PMVPMAOH (20% mole ratio) using different infiltration methods: a) by filtration, and, b–d) by capillary force.

areas were observed after examining different regions of the sample prepared by capillary force infiltration. Also, the 3D XRM images (Figure 9a–e and Supporting Information, Figure S16) displayed the virtual slices through the imaging volume and the surface view of the structure, revealing the three-dimensionally continuous and homogeneous ordered porous structure in this material. While X-ray microcomputed tomography (micro-CT) has been used to characterize inverse opals with 16 μm resolution,[34] this demonstration showed the feasibility of using nanoscale 3D XRM for the visualization of the 3D morphology of 3DOM materials down to 50 nm resolution (16 nm voxels), representing up to three orders of magnitude improved resolution from the previous micro-CT experiments.[35]

The CO_2 absorption/desorption profiles of the material synthesized by using capillary forces to infiltrate the colloidal crystal are given in Table 1 (entry 12) and the Supporting Information (Figure S22). The overall rate of CO_2 capture and release was 1.7 times greater, and the swing size was 3.2 times larger than for the Excellion membrane. This sample made using the infiltration method by capillary force also

2.4. Influence of Different Infiltration Methods

During the infiltration by vacuum filtration, the PMMA colloidal crystals templates were crushed to powders, causing many defects in their ordered crystal structures. During polymerization, the voids between the grains are filled with non-porous polymers. As shown in the SEM image in **Figure 8**a, although the pores can be observed throughout the sample, the existence of a few regions of non-porous polymers can be seen on their surfaces. In addition, the nanoscale 3D X-ray microscopy (XRM) was employed to non-destructively resolve the 3D structures of this material, and the results are shown in **Figure 9**f and the Supporting Information, Figure S15. In the 2D virtual orthogonal slice of the 3D dataset, inhomogeneous structures were observed with some areas laced with the honeycomb structure, while others only had dense bulk matter.

To reduce the defects in the crosslinked polymeric materials, a different infiltration method was used to give bulk templates instead of powder templates. The bulk PMMA colloidal crystals templates were directly used for the infiltration, and the precursor solution was poured over the material, and allowed to infiltrate the pores by capillary forces.[33] Since the bulk PMMA colloidal crystals templates have fewer defects than the powder templates, the resulting samples would have better interconnectivity between the pores. The SEM images in Figure 8b–d show that no non-porous

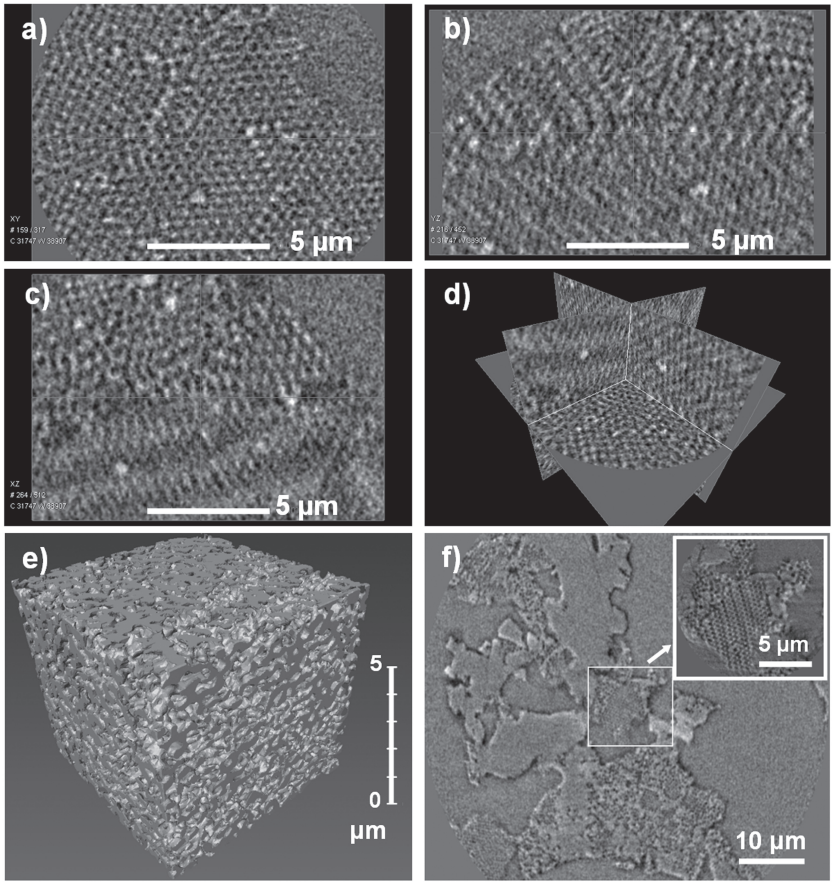

Figure 9. 3D XRM images of the 3DOM polymeric materials prepared by PMMA colloidal crystal templating with VBTMAOH and PMVPMAOH (20% mole ratio) using different infiltration methods (by capillary force (a–e) and by filtration (f)): a–c) the virtual slices through the imaging volume, d) the intersection between viewing planes, e) the surface view of the structure, and, f) the 2D virtual orthogonal slice of the 3D dataset. The inset in (f) is an enlarged image of a selected area.

had a larger swing size compared to the samples made using filtration, which could originate from the better interconnectivity between the pores.

2.5. 3DOM Polymer Films by PS Colloidal Crystals Templating

By using the multilayered colloidal crystal films as the templates,[36] the crosslinked macroporous polymer films can be prepared. The thickness of these films is typically in the micrometer range, which is much thinner than the bulk materials that are in the millimeter range. These thin porous films will have greater fraction of pores located near the surfaces, so the gas will travel a much shorter distance before reaching these pores in the center of the material compared to the bulk porous materials, which should facilitate the fluid transport kinetics through the pores.

The vertical deposition method[14] was used to prepare the film-shaped colloidal crystals. The monodisperse PS latex was prepared by the surfactant-free emulsion polymerization of styrene, and then the colloidal PS spheres were assembled onto the surface of a vertically aligned glass slide to form a continuous film during the evaporation process through convective self-assembly.[17c,37] The film exhibited a nacre color under white light due to Bragg diffraction of visible light, indicating the ordered photonic crystal structures (the inset of **Figure 10**a).[38] The SEM images show the ordered fcc packing structure of the resulting samples with average PS particle size of 278 nm (Figure 10a–c).

The films of the PS colloidal crystals were sandwiched between two glass slides, and infiltrated with an aqueous solution of VBTMACl and PMVPMACl (20% molar ratio). After polymerization, the resulting polymer films were washed with THF/acetone to dissolve the PS particles, generating an interconnected macroporous structure with an average pore size of ca. 220 nm (Figure 10d–f). The fast Fourier transform (FFT) of the SEM image (the inset in Figure 10f) showed first- and higher-order spots, revealing the regular pattern of the uniform pores.[39] Finally, the chloride anions in the porous polymer films were then ion-exchanged with KOH in methanol or aqueous solution to obtain the porous polymer containing quaternary ammonium cations hydroxide anions. After ion exchange, the macropores and the windows between the pores were preserved (Figure 10g–i). The macropores have an average size of 170 nm, and the pore walls were thicker than the same samples before ion exchange, which might be due to the swelling and deformation of polymer scaffolds containing the hydroxide counterion. After ion exchange with KOH, the chlorine contents of the polymer films were reduced to trace amounts as measured by elemental analysis; while for the previous bulk samples, the chlorine content was still 1.4–4.3% after ion exchange under the same conditions (Supporting Information, Table S1). Thus, the film materials have much better ion-exchange efficiency than the bulk materials, probably due to their better fluid diffusion properties.

When exposed to the humidity swing cycle, the swing size of the 3DOM polymer films was 4.4 times larger than the Excellion membrane, and the kinetics were 2.1 times faster, as shown in Table 1 (entry 13) and the Supporting Information (Figure S23). This sample showed the highest swing size (0.57 mmol g^{-1}) among all the studied samples, which could be because of the thinner film sample enable more active sites inside this material to interact with CO_2. In all cases the CO_2 capture occurs by chemisorption, and it is worth noting that there were ca. 2.3 mmol g^{-1} of the quaternary ammonium sites potentially available for CO_2 capture, as measured by elemental analysis (Supporting Information, Part G). This reveals a utilization efficiency of ca. 50%, which is presumably because some of the quaternary ammonium groups were embedded inside the crosslinked polymers and inaccessible to outside gas molecules.

It is important to bear in mind that these CO_2 capture experiments were performed under near ambient conditions (i.e., with ca. 400 parts per million (ppm) of CO_2), and that the swing size was recorded as the amount of CO_2 captured upon reaching the maximum absorption attained in the humidity swing. This is because in this work, the swing behavior (i.e., kinetics and cyclibility) under near ambient conditions was the focus. However, the low partial pressure of CO_2 of ca. 400 ppm makes the swing size smaller

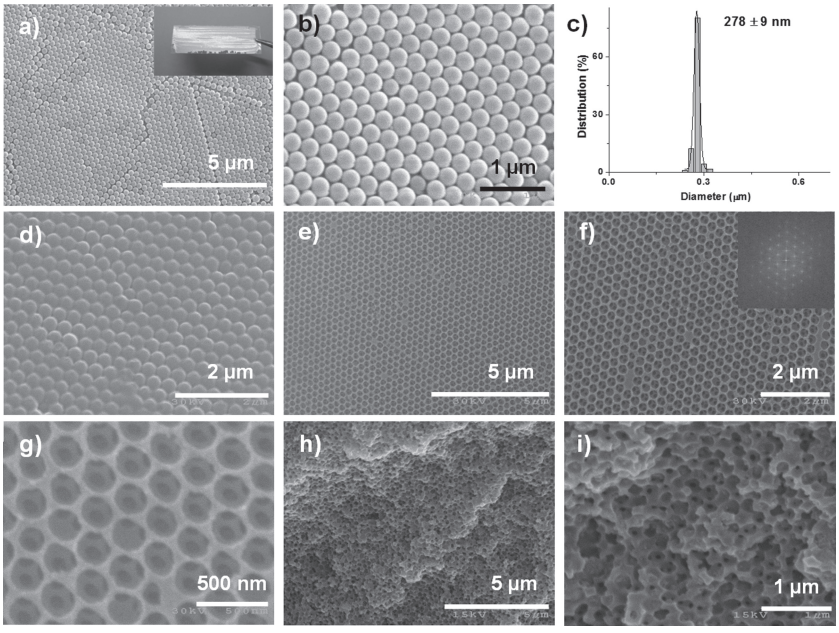

Figure 10. SEM images of PS colloidal crystals films (a,b), the particle size histogram with a Gaussian size distribution fit (solid line) of PS colloidal crystals films (c), and the SEM images of the 3DOM polymer films prepared by colloidal crystal templating with VBTMACl and PMVPMACl (20% mole ratio): after infiltration and polymerization (d); after removal of the PS colloidal crystal templates (e,f,g); and, after ion exchange in KOH/methanol solution (h,i). The inset in (a) is a photo of the PS colloidal crystals film on a glass slide under white light. The inset in (f) is the fast Fourier transform of the SEM image in (f).

than the maximum uptake or capacity. Therefore, despite the fact that the swing size of ca. 0.6 mmol g^{-1} is smaller than the 1–4 mmol g^{-1} seen in CO_2 absorption isotherms at 1 atm of CO_2 after prior treatments of the sorbents by vacuumization or heating,[40] these humidity swing materials perform comparably or even better than typical porous materials at low concentrations of CO_2.

3. Conclusions

In summary, by using PMMA or PS latex particle based colloidal crystals as the templates, crosslinked polymer networks with 3DOM structures were successfully synthesized by the polymerization of water-soluble cationic monomers and dicationic crosslinkers. The dicationic crosslinker was stable under highly basic conditions, and preserved the highly porous structure. By directly using the hydroxide-containing mononmer and dicationic crosslinker, the structures had less shrinkage compared to those prepared from the chloride containing monomer and dicationic crosslinker, followed by the hydroxide ion exchange. Infiltration of the polymer precursor solution into the colloidal crystal template by capillary force reduced the defects in the porous structure compared to infiltration under partial vacuum, as confirmed by SEM and 3D XRM characterizations. The colloidal crystal templating method was versatile since bulk or film porous polymeric materials could be obtained with thicknesses between millimeters and micrometers. These differences in the thickness of the materials are achieved simply by varying the thickness of the colloidal crystals template. The thin porous films showed better ion-exchange properties than their bulk counterparts, as revealed by elemental analysis. The quaternary ammonium hydroxide groups in the porous polymers allow the material to be used for reversible capture and release of CO_2 by humidity swing. Compared to Excellion membranes, a commercially available standard for CO_2 absorption/desorption by the humidity swing, the colloidal crystal templated materials improved the rates of CO_2 absorption/desorption by a factor of 2–5, and the swing size by a factor of 2–4. The synthetic strategy developed in this work sheds a new light on the design of well-defined structures and controlled properties of porous materials by colloidal crystal templating, which can be used for CO_2 capture and other potential applications.

Supporting Information

Supporting Information is available from the Wiley Online Library or from the author.

Acknowledgements

The authors thank Joseph P. Suhan for his help on the SEM and TEM measurements. They acknowledge NSF support (CHE-1039870 and DMR-0969301).

Received: January 31, 2013
Revised: February 23, 2013
Published online: April 19, 2013

[1] a) Y. N. Xia, B. Gates, Y. D. Yin, Y. Lu, *Adv. Mater.* **2000**, *12*, 693; b) F. Li, D. P. Josephson, A. Stein, *Angew. Chem., Int. Ed.* **2011**, *50*, 360.
[2] a) P. N. Pusey, W. Vanmegen, *Nature* **1986**, *320*, 340; b) D. Frenkel, *Physica A* **1999**, *263*, 26.
[3] a) V. L. Colvin, *MRS Bull.* **2001**, *26*, 637; b) Y. J. Lee, P. V. Braun, *Adv. Mater.* **2003**, *15*, 563; c) J. D. Joannopoulos, P. R. Villeneuve, S. H. Fan, *Nature* **1997**, *386*, 143; d) S. A. Rinne, F. Garcia-Santamaria, P. V. Braun, *Nat. Photonics* **2008**, *2*, 52.
[4] a) S. A. Asher, V. L. Alexeev, A. V. Goponenko, A. C. Sharma, I. K. Lednev, C. S. Wilcox, D. N. Finegold, *J. Am. Chem. Soc.* **2003**, *125*, 3322; b) A. C. Sharma, T. Jana, R. Kesavamoorthy, L. J. Shi, M. A. Virji, D. N. Finegold, S. A. Asher, *J. Am. Chem. Soc.* **2004**, *126*, 2971; c) J.-T. Zhang, L. Wang, J. Luo, A. Tikhonov, N. Kornienko, S. A. Asher, *J. Am. Chem. Soc.* **2011**, *133*, 9152; d) J. H. Holtz, S. A. Asher, *Nature* **1997**, *389*, 829.
[5] M. R. Newton, A. K. Bohaty, H. S. White, I. Zharov, *J. Am. Chem. Soc.* **2005**, *127*, 7268.
[6] a) Y. J. Zhang, S. P. Wang, M. Eghtedari, M. Motamedi, N. A. Kotov, *Adv. Funct. Mater.* **2005**, *15*, 725; b) S.-W. Choi, Y. Zhang, Y. Xia, *Langmuir* **2010**, *26*, 19001.
[7] a) D. Wu, F. Xu, B. Sun, R. Fu, H. He, K. Matyjaszewski, *Chem. Rev.* **2012**, *112*, 3959; b) A. Stein, R. C. Schroden, *Curr. Opin. Solid State Mater. Sci.* **2001**, *5*, 553; c) O. D. Velev, A. M. Lenhoff, *Curr. Opin. Colloid Interface Sci.* **2000**, *5*, 56; d) X. S. Zhao, F. B. Su, Q. F. Yan, W. P. Guo, X. Y. Bao, L. Lv, Z. C. Zhou, *J. Mater. Chem.* **2006**, *16*, 637; e) J. Lee, J. Kim, T. Hyeon, *Adv. Mater.* **2006**, *18*, 2073.
[8] F. Meseguer, A. Blanco, H. Miguez, F. Garcia-Santamaria, M. Ibisate, C. Lopez, *Colloid Surf. A* **2002**, *202*, 281.
[9] A. Stein, F. Li, N. R. Denny, *Chem. Mater.* **2008**, *20*, 649.
[10] O. D. Velev, E. W. Kaler, *Adv. Mater.* **2000**, *12*, 531.
[11] a) K. E. Davis, W. B. Russel, W. J. Glantschnig, *Science* **1989**, *245*, 507; b) M. Holgado, F. Garcia-Santamaria, A. Blanco, M. Ibisate, A. Cintas, H. Miguez, C. J. Serna, C. Molpeceres, J. Requena, A. Mifsud, F. Meseguer, C. Lopez, *Langmuir* **1999**, *15*, 4701; c) R. Mayoral, J. Requena, J. S. Moya, C. Lopez, A. Cintas, H. Miguez, F. Meseguer, L. Vazquez, M. Holgado, A. Blanco, *Adv. Mater.* **1997**, *9*, 257.
[12] N. V. Dziomkina, G. J. Vancso, *Soft Matter* **2005**, *1*, 265.
[13] P. N. Pusey, W. Vanmegen, P. Bartlett, B. J. Ackerson, J. G. Rarity, S. M. Underwood, *Phys. Rev. Lett.* **1989**, *63*, 2753.
[14] a) P. Jiang, J. F. Bertone, K. S. Hwang, V. L. Colvin, *Chem. Mater.* **1999**, *11*, 2132; b) B. Lange, F. Fleischhaker, R. Zentel, *Phys. Status Solidi A* **2007**, *204*, 3618; c) A. S. Dimitrov, K. Nagayama, *Langmuir* **1996**, *12*, 1303.
[15] a) R. C. Schroden, M. Al-Daous, S. Sokolov, B. J. Melde, J. C. Lytle, A. Stein, M. C. Carbajo, J. T. Fernandez, E. E. Rodriguez, *J. Mater. Chem.* **2002**, *12*, 3261; b) R. C. Schroden, M. Al-Daous, C. F. Blanford, A. Stein, *Chem. Mater.* **2002**, *14*, 3305.
[16] a) S. H. Park, D. Qin, Y. N. Xia, *Adv. Mater.* **1998**, *10*, 1028; b) S. H. Park, Y. N. Xia, *Langmuir* **1999**, *15*, 266.
[17] a) S. H. Park, Y. N. Xia, *Chem. Mater.* **1998**, *10*, 1745; b) B. Gates, Y. D. Yin, Y. N. Xia, *Chem. Mater.* **1999**, *11*, 2827; c) P. Jiang, K. S. Hwang, D. M. Mittleman, J. F. Bertone, V. L. Colvin, *J. Am. Chem. Soc.* **1999**, *121*, 11630.
[18] S. A. Johnson, P. J. Ollivier, T. E. Mallouk, *Science* **1999**, *283*, 963.
[19] S. H. Park, Y. N. Xia, *Adv. Mater.* **1998**, *10*, 1045.
[20] H. Fudouzi, Y. N. Xia, *Adv. Mater.* **2003**, *15*, 892.
[21] X. Zhang, W. Yan, H. Yang, B. Liu, H. Li, *Polymer* **2008**, *49*, 5446.
[22] R. B. Pernites, E. L. Foster, M. J. L. Felipe, M. Robinson, R. C. Advincula, *Adv. Mater.* **2011**, *23*, 1287.
[23] H. C. Liou, P. S. Ho, A. McKerrow, *J. Polym. Sci., Part B: Polym. Phys.* **1998**, *36*, 1383.
[24] a) S. Chu, *Science* **2009**, *325*, 1599; b) M. R. Allen, D. J. Frame, C. Huntingford, C. D. Jones, J. A. Lowe, M. Meinshausen,

N. Meinshausen, *Nature* **2009**, *458*, 1163; c) C. D. Thomas, A. Cameron, R. E. Green, M. Bakkenes, L. J. Beaumont, Y. C. Collingham, B. F. N. Erasmus, M. F. de Siqueira, A. Grainger, L. Hannah, L. Hughes, B. Huntley, A. S. van Jaarsveld, G. F. Midgley, L. Miles, M. A. Ortega-Huerta, A. T. Peterson, O. L. Phillips, S. E. Williams, *Nature* **2004**, *427*, 145; d) C. W. Jones, E. J. Maginn, *ChemSusChem* **2010**, *3*, 863.

[25] a) S. Choi, J. H. Drese, C. W. Jones, *ChemSusChem* **2009**, *2*, 796; b) D. M. D'Alessandro, B. Smit, J. R. Long, *Angew. Chem., Int. Ed.* **2010**, *49*, 6058.

[26] a) S. Choi, J. H. Drese, P. M. Eisenberger, C. W. Jones, *Environ. Sci. Technol.* **2011**, *45*, 2420; b) K. S. Lackner, *Science* **2003**, *300*, 1677; c) M. S. Abd Rahaman, L.-H. Cheng, X.-H. Xu, L. Zhang, H.-L. Chen, *Renewable Sustainable Energy Rev.* **2011**, *15*, 4002; d) C. Gebald, J. A. Wurzbacher, P. Tingaut, T. Zimmermann, A. Steinfeld, *Environ. Sci. Technol.* **2011**, *45*, 9101.

[27] a) K. S. Lackner, *Eur. Phys. J. Spec. Top.* **2009**, *176*, 93; b) T. Wang, K. S. Lackner, A. Wright, *Environ. Sci. Technol.* **2011**, *45*, 6670.

[28] H. K. He, W. W. Li, M. J. Zhong, D. Konkolewicz, D. C. Wu, K. Yaccato, T. Rappold, G. Sugar, N. E. David, K. Matyjaszewski, *Energy Environ. Sci.* **2013**, *6*, 488.

[29] Y. Chung-li, J. W. Goodwin, R. H. Ottewill, *Prog. Colloid Polym. Sci.* **1976**, *60*, 163.

[30] F. Marlow, Muldarisnur, P. Sharifi, R. Brinkmann, C. Mendive, *Angew. Chem., Int. Ed.* **2009**, *48*, 6212.

[31] L. V. Woodcock, *Nature* **1997**, *385*, 141.

[32] J. X. Zhu, M. Li, R. Rogers, W. Meyer, R. H. Ottewill, W. B. Russell, P. M. Chaikin, *Nature* **1997**, *387*, 883.

[33] J. Wang, Y. Cao, Y. Feng, F. Yin, J. Gao, *Adv. Mater.* **2007**, *19*, 3865.

[34] a) S.-W. Choi, Y. Zhang, S. Thomopoulos, Y. Xia, *Langmuir* **2010**, *26*, 12126; b) M.-Y. Bai, C. H. Moran, L. Zhang, C. Liu, Y. Zhang, L. V. Wang, Y. Xia, *Adv. Funct. Mater.* **2012**, *22*, 764.

[35] W. K. Epting, J. Gelb, S. Litster, *Adv. Funct. Mater.* **2012**, *22*, 555.

[36] B. Hatton, L. Mishchenko, S. Davis, K. H. Sandhage, J. Aizenberg, *Proc. Natl. Acad. Sci. USA* **2010**, *107*, 10354.

[37] Z. C. Zhou, X. S. Zhao, *Langmuir* **2005**, *21*, 4717.

[38] A. Gil, M. Vaupel, F. Guitian, D. Moebius, *J. Mater. Chem.* **2007**, *17*, 2434.

[39] L. Billon, M. Manguian, V. Pellerin, M. Joubert, O. Eterradossi, H. Garay, *Macromolecules* **2009**, *42*, 345.

[40] a) M. Zhong, S. Natesakhawat, J. P. Baltrus, D. Luebke, H. Nulwala, K. Matyjaszewski, T. Kowalewski, *Chem. Commun.* **2012**, *48*, 11516; b) P. Pachfule, B. K. Balan, S. Kurungot, R. Banerjee, *Chem. Commun.* **2012**, *48*, 2009; c) J. C. Hicks, J. H. Drese, D. J. Fauth, M. L. Gray, G. Qi, C. W. Jones, *J. Am. Chem. Soc.* **2008**, *130*, 2902; d) H. Furukawa, O. M. Yaghi, *J. Am. Chem. Soc.* **2009**, *131*, 8875; e) G.-P. Hao, W.-C. Li, D. Qian, A.-H. Lu, *Adv. Mater.* **2010**, *22*, 853.